A SEMI-ANALYTICAL METHOD FOR DETERMINING THE ENERGY RELEASE RATE OF CRACKS IN ADHESIVELY-BONDED SINGLE-LAP COMPOSITE JOINTS

Chihdar Yang, Wenjun Sun, John S. Tomblin

Department of Aerospace Engineering
Wichita State University
Wichita, KS 67260-0044

and

Stanley S. Smeltzer III

Mechanics of Structures and Materials Branch
NASA Langley Research Center
Hampton, VA 23681-2199

August 30, 2005

Please direct correspondence to:

Dr. Chihdar (Charles) Yang
Department of Aerospace Engineering
Campus Box 44
Wichita State University
Wichita, KS 67260-0044
Email: charles.yang@wichita.edu
Tel.: 316.978.6312
Fax: 316.978.3307

ABSTRACT

A semi-analytical method for determining the strain energy release rate due to a prescribed interface crack in an adhesively-bonded, single-lap composite joint subjected to axial tension is presented. The field equations in terms of displacements within the joint are formulated by using first-order shear deformable, laminated plate theory together with kinematic relations and force equilibrium conditions. The stress distributions for the adherends and adhesive are determined after the appropriate boundary and loading conditions are applied and the equations for the field displacements are solved. Based on the adhesive stress distributions, the forces at the crack tip are obtained and the strain energy release rate of the crack is determined by using the virtual crack closure technique (VCCT). Additionally, the test specimen geometry from both the ASTM D3165 and D1002 test standards are utilized during the derivation of the field equations in order to correlate analytical models with future test results. The system of second-order differential field equations is solved to provide the adherend and adhesive stress response using the symbolic computation tool, Maple 9. Finite element analyses using *J*-integral as well as VCCT were performed to verify the developed analytical model. The finite element analyses were conducted using the commercial finite element analysis software ABAQUS™. The results determined using the analytical method correlated well with the results from the finite element analyses.

KEY WORDS: adhesively-bonded joint, laminated plate theory, composite joint, strain energy release rate, virtual crack closure technique (VCCT), fracture mechanics

NOMENCLATURE

P:	applied tensile force per unit width, N/m
u^U, u^L:	x-directional displacement, m
u^o, u^{oU}, u^{oL}:	mid-plane x-directional displacement, m
ψ, ψ^U, ψ^L:	bending slope, radians
w, w^U, w^L:	z-directional displacement, m
N_x, $N_x{}^U$, $N_x{}^L$:	normal stress resultants per unit width, kN/m
M_y, $M_y{}^U$, $M_y{}^L$:	bending moment per unit width, kN
Q_z, $Q_z{}^U$, $Q_z{}^L$:	transverse shear stress resultant per unit width, kN/m
A_{11}, $A_{11}{}^U$, $A_{11}{}^L$:	in-plane modulus per unit width, kN/m
A_{55}, $A_{55}{}^U$, $A_{55}{}^L$:	transverse modulus per unit width, kN/m
B_{11}, $B_{11}{}^U$, $B_{11}{}^L$:	coupling modulus per unit width, kN
D_{11}, $D_{11}{}^U$, $D_{11}{}^L$:	flexural modulus per unit width, kNm
k_s, $k_s{}^U$, $k_s{}^L$:	shear correction factor
τ_a:	adhesive shear stress, kPa
q_a, σ_z:	adhesive peel stress, kPa
h^U, h^L:	adherend thickness, m
η:	adhesive thickness, m
σ_x, σ_y:	adhesive normal stress, kPa
ε_x, ε_y, ε_z, γ_{xz}:	adhesive strain
E_a:	Young's modulus of adhesive, kPa
G_a:	shear modulus of adhesive, kPa
ν_a:	Poisson's ratio of adhesive
a:	length of prescribed crack, m
b:	length of virtual crack extension, m
l_o:	overlap length before crack is initiated, m
l_n:	notch length of ASTM D3165 specimen, m
N_C, M_C, Q_C:	crack tip forces
W:	work required to close crack propagation b per unit joint width, N
G_T:	total strain energy release rate, N/m
F_{xf}, F_{yf}, F_{xg}, F_{yg}:	crack tip forces from finite element model, N
J:	J-integral value

INTRODUCTION

Advanced composite materials have been widely used due to their high strength-to-weight ratio and excellent corrosion resistance. In many applications, bolted joints have been replaced by adhesively-bonded joints because of the weight penalty and corrosion problems associated with bolted joints. However, the geometric discontinuity present at the ends of an adhesively-bonded joint results in peak shear and normal (peel) stresses in the adhesive layer that typically occur near the adhesive to adherend interface. The stress concentration caused by the discontinuity often results in local yielding and further develops into crack initiation. In a research study conducted by Yang *et al*. [1] on adhesively-bonded joints, they concluded that the fracture mechanics approach would be an effective method for predicting the load carrying capacity of a bonded joint.

Earlier studies of adhesively-bonded joints can be found in the extensive reviews given by Kutscha [2], Kutscha and Hofer [3], Matthews *et al*. [4], and Vinson [5]. Yang and Pang [6] derived an analytical model that provided the stress distributions of adhesively-bonded single-lap composite joints subjected to axial tension. Huang *et al*. [7] and Yang *et al*. [8] also derived an elastic-plastic model for adhesively-bonded single-lap composite joints. Important capabilities included in their approaches were the asymmetry of the adherend laminates as well as the effects due to transverse shear deformation.

An existing crack is usually assumed in a joint when conducting a fracture analysis. Krueger [9] described the virtual crack closure technique (VCCT), including its history, approach, and applications, in conjunction with finite element analysis in a report published in 2002. Davidson *et al*. [10-13] published a series of papers that employed the classical plate theory version of the VCCT to predict the strain energy release rate of mixed-mode delamination

in composite laminates. A crack-tip force method was derived by Park and Sankar [14] to compute the strain energy release rate in delaminated beams and plates. Kim *et al*. [15] proposed a simplified method for determining the strain energy release rate of free edge delamination in composites using the classical laminated plated theory. Finite element methods play a significant role in structural analysis and have been widely used to study the adhesively-bonded composite joint. Wang *et al*. [16] applied the VCCT to calculate the strain energy release rate of cracked composite panels with nonlinear deformation. Wei *et al*. [17] presented an improved VCCT to determine the energy release rate using a three-step analysis. Yang *et al.* [1] developed finite element models using the finite element software, ABAQUS™, to estimate the *J*-integral of an adhesively-bonded joint with a crack.

Although finite element analysis methods are capable of solving problems with varying material types and complicated geometrical configurations, analytical solutions offer performance and solution advantageous, especially when performing parametric analyses and optimization. The objective of the present paper is to describe a semi-analytical fracture mechanics method that can be used to determine the strain energy release rate due to a prescribed crack in an adhesively-bonded single-lap composite joint. The prescribed crack is assumed to be present at the location of peak stress in the overlap region, usually at the corners of the adhesive adjacent to the continuous adherend. Additionally, the strain energy release rate calculated using this method can be applied to configurations with adhesive or adhesive/adherend interfaces as a failure criterion given the same mixed-mode critical strain energy release rate exists in the subject joint to account for the adhesive cohesion or adhesion failure. Linear elastic material properties as well as small displacements are assumed for both the adhesive and adherends in order to make the analytical approach feasible. Due to the fact that the geometric nonlinearity

during the joint deformation is not considered, the analytical model is more accurate when analyzing joints with stiffer and/or thicker adherends.

In the remaining sections, the displacement fields and stress distributions of adhesively-bonded single-lap composite joints with a prescribed interface crack under tension are determined analytically using laminated anisotropic plate theory. After the virtual crack extension is applied, the crack tip forces are calculated based on the adhesive stress distributions. The strain energy release rate is then calculated using the VCCT. ASTM D3165 [18] and ASTM D1002 [19] specimen geometries are used in the model derivations. The semi-analytical solutions are determined using the symbolic computation tool Maple 9 [20]. Results from the analytical model are verified by finite element analysis using ABAQUS™ 6.3 [21, 22].

ANALYTICAL DEVELOPMENT OF FIELD EQUATIONS FOR THE CALCULATION OF ENERGY RELEASE RATES

The details of the semi-analytical method for determining the strain energy release rate of adhesively-bonded single-lap composite joints with a prescribed interface crack are now given. Based on the laminated plate theory version of Irwin's virtual crack method [9], the strain energy release rate is derived in terms of the forces and moment at the crack tip, N_c, Q_c, and M_c. These forces and moments at the crack tip are determined from the linear elastic shear and peel stress distributions in the adhesive. Therefore, a description of the stress state in the pre- and post-cracked specimen geometry is required before an estimate of the strain energy release rate can be obtained.

ASTM D3165 Stress Model

A summary of the basic methodology used by the authors to derive the equations for determining the required stress and displacement fields in an adhesively-bonded joint are

presented in the present section. The details of the method used to determine the displacement, strain, and stress fields in an adhesively bonded joint are available in the previous report by Yang and Pang [6]. Shown in Figure 1 is an adhesively-bonded single-lap joint with the standard geometry of an ASTM D3165 specimen and an applied tensile load P per unit width. The specimen geometry is divided into five regions to aid in the derivation of model equations. Region 3 is the bonded joint overlap area where the applied mechanical loads are transferred from one adherend to the other, and is also the area for which the joint strength is typically based.

The generalized field equations for the adherends and adhesive are the same for all the three regions with an adhesive layer. The behavior of the adherends is described by the laminated anisotropic plate theory and the adhesive is assumed to behave as an elastic, isotropic material. The displacement fields for the upper and lower adherends can be written as follows:

$$u^U = u^{oU}(x) + z^U \psi^U(x) \quad \textbf{(1)}$$

$$u^L = u^{oL}(x) + z^L \psi^L(x) \quad \textbf{(2)}$$

$$w^U = w^U(x) \quad \textbf{(3)}$$

$$w^L = w^L(x) \quad \textbf{(4)}$$

where displacements in the axial (x) direction are given by u, displacements in the transverse (z) direction are given by w, the superscripts U and L denote the upper and lower adherends, respectively, superscript o represents the mid-plane displacement, and ψ is the corresponding bending slope. The normal stress resultant per unit width, N_x, bending moment per unit width, M_y, and transverse shear stress resultant per unit width, Q_z, are expressed as

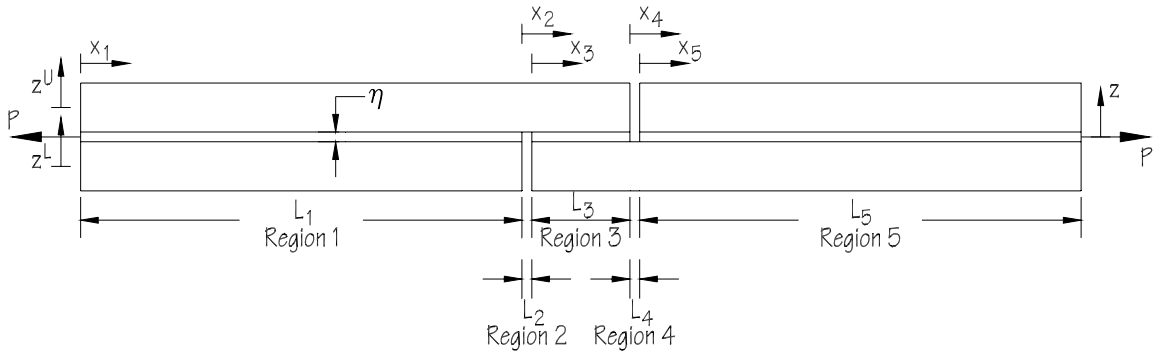

Figure 1. *ASTM D3165 specimen configuration and coordinate systems.*

$$N_x = A_{11}\frac{du^o(x)}{dx} + B_{11}\frac{d\psi(x)}{dx} \tag{5}$$

$$M_y = B_{11}\frac{du^o(x)}{dx} + D_{11}\frac{d\psi(x)}{dx} \tag{6}$$

$$Q_z = k_s A_{55}\left[\psi(x) + \frac{dw(x)}{dx}\right] \tag{7}$$

where k_s is the shear correction factor and the A_{ij}, B_{ij}, and D_{ij} terms are taken from the common extensional, bending, and extensional-bending coupling stiffness matrices from the laminated plate theory [23]. In order to establish the equations of equilibrium, a free body diagram of a differential element from the overlap region is shown in Figure 2. The equations for force equilibrium of the upper adherend are given as:

$$\frac{dN_x^U}{dx} = -\tau_a \tag{8}$$

$$\frac{dM_y^U}{dx} = Q_z^U + \frac{h^U}{2}\tau_a \tag{9}$$

$$\frac{dQ_z^U}{dx} = q_a \tag{10}$$

where τ_a and q_a are the shear and peel stresses of the adhesive, respectively, and h^U is the thickness of the upper adherend. Three equilibrium equations can be obtained for the lower adherend in a similar fashion to show:

$$\frac{dN_x^L}{dx} = \tau_a \tag{11}$$

$$\frac{dM_y^L}{dx} = Q_z^L + \frac{h^L}{2}\tau_a \tag{12}$$

$$\frac{dQ_z^L}{dx} = -q_a \tag{13}$$

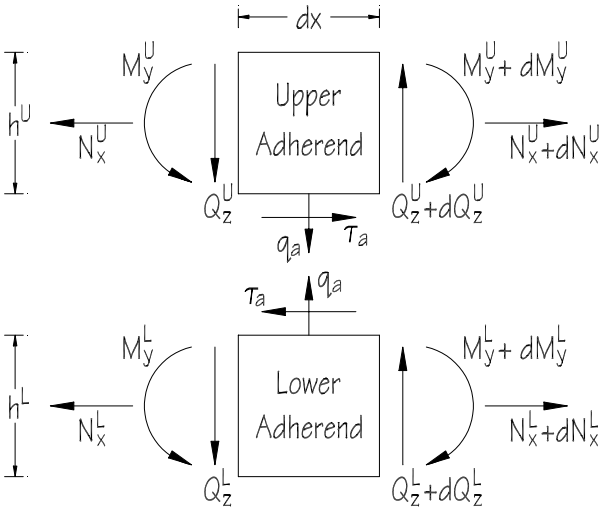

Figure 2. *Free body diagram and sign conventions.*

Using the kinematics of the adherends and assuming a perfect bond between the adhesive and the adherend surfaces, the adhesive strains are related to the bottom surface of the upper adherend and the top surface of the lower adherend. In terms of the displacement field of the two adherends, the adhesive strains in the traditional sign convention with *x*, *y*, *z* subscripts can be written as:

$$\gamma_{xz} = \frac{1}{\eta}\left[\left(u^{oU} - u^{oL}\right) - \left(\frac{h^U}{2}\psi^U + \frac{h^L}{2}\psi^L\right)\right] + \frac{1}{2}\left(\frac{dw^L}{dx} + \frac{dw^U}{dx}\right) \tag{14}$$

$$\varepsilon_x = \frac{1}{2}\frac{d}{dx}\left[\left(u^{oL} + u^{oU}\right) + \left(\frac{h^L}{2}\psi^L - \frac{h^U}{2}\psi^U\right)\right] \tag{15}$$

$$\varepsilon_z = \frac{1}{\eta}\left(w^U - w^L\right) \tag{16}$$

where η is the adhesive thickness, and h^U and h^L are the thickness of the upper and lower adherends, respectively. Assuming a condition of plane-strain, the adhesive stresses can be obtained as:

$$\sigma_x = \frac{E_a}{(1+\nu_a)(1-2\nu_a)}\left[(1-\nu_a)\varepsilon_x + \nu\,\varepsilon_z\right] \tag{17}$$

$$\sigma_y = \frac{\nu E_a}{(1+\nu_a)(1-2\nu_a)}\left(\varepsilon_x + \varepsilon_z\right) \tag{18}$$

$$q_a = \sigma_z = \frac{E_a}{(1+\nu_a)(1-2\nu_a)}\left[\nu\,\varepsilon_x + (1-\nu_a)\varepsilon_z\right] \tag{19}$$

$$\tau_a = -G_a\,\gamma_{xz} \tag{20}$$

As previously noted, τ_a and q_a are the shear and peel stresses of the adhesive, respectively, and their sign conventions are shown in Figure 2. E_a is the Young's modulus, ν_a is the Poisson's ratio, and G_a is the shear modulus of the adhesive.

Substituting the stress resultants in Equations (5) - (7) for the upper and lower adherends along with the adhesive stresses in Equations (19) and (20) into Equations (8) - (13), six coupled second-order ordinary differential equations with six unknowns u^{oU}, ψ^U, w^U, u^{oL}, ψ^L, and w^L are obtained for each of Regions 1, 3, and 5. In Region 2, only the upper adherend is present without any adhesive stresses. Therefore, the force equilibrium conditions in Region 2 are similar to those in Equations (8) – (10) but without the adhesive stresses, τ_a and q_a,

$$\frac{dN_x^U}{dx} = 0 \tag{21}$$

$$\frac{dM_y^U}{dx} = Q_z^U \tag{22}$$

$$\frac{dQ_z^U}{dx} = 0 \tag{23}$$

Substituting the stress resultants in Equations (5) - (7) of the upper adherend into Equations (21) – (23), three coupled second-order ordinary differential equations with three variables u^{oU}, ψ^U, and w^U are obtained for Region 2. Applying the similar approach to Region 4 yields another three coupled second-order ordinary differential equations with three variables u^{oL}, ψ^L, and w^L.

The overall system of governing equations, including all five regions, contains twenty-four second-order ordinary differential equations with twenty-four unknown variables. A total of forty-eight boundary conditions are obtained at the two ends of each Region based on either continuity or applied force conditions. The symbolic solver Maple 9 was used to solve the system of equations and obtain the displacement, strain, and stress fields.

Strain Energy Release Rate Calculation

Once the stress, strain, and displacement fields are known in the adhesively-bonded single-lap composite joints, the virtual crack closure technique (VCCT) is applied to estimate the strain energy release rate of the joint with a prescribed interface crack. According to linear elastic fracture mechanics, the energy released from the propagation of a small crack is equivalent to the work needed to close that small crack propagation [16].

When a crack is initiated, it usually starts at a location of high stress concentration. For the ASTM D3165 specimen configuration shown in Figure 1, the critical areas are located at the upper left and lower right corners of the adhesive layer in Region 3. In deriving an expression for the strain energy release rate, a joint is assumed to have an overlap length l_o, a notch size l_n,

and a crack of length a that is located at the lower right adhesive/adherend interface. Due to the anti-symmetry of the joint, only the right half of the joint, as shown in Figure 3, is used for the strain energy release rate calculation. The displacement of the crack tip C after a load is applied can be determined using the stress model previously described and a Region 3 length of $L_3 = l_o - 2a$ and Regions 2 and 4 lengths of $L_2 = L_4 = l_n + a$. In the stress formulation, two boundary conditions used for solving the field equations are that the displacements in both the x and z directions of the left end of the joint ($x_1 = 0$) are zero. Because only the right-half of the joint is used in the strain energy release rate calculation, the center point O of the joint, as shown in Figure 3, is used as the reference point to avoid double-counting the effects due to the crack. Both the displacements in x and z directions, u and w, in the strain energy release rate calculation are relative displacements to point O. However, the absolute bending slope, ψ, is used directly for the strain energy release rate calculation. According to the displacement fields for the upper and the lower adherends, the relative displacements of the crack tip C to the reference point O are obtained using the stress model and a joint with a central overlap length $L_3 = l_o - 2a$ and notch lengths $L_2 = L_4 = l_n + a$, i.e.

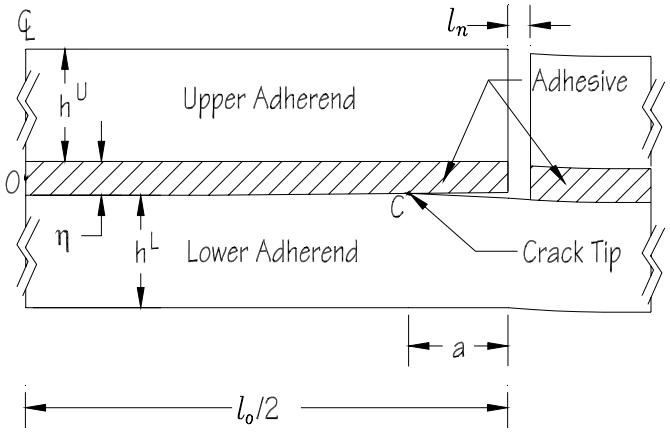

Figure 3. *A joint of central overlap length l with a prescribed interface crack of length a.*

$$u_{C,O} = u^{oL}\,|_{x_3=l_o-2a} + \frac{h^L}{2}\psi^L\,|_{x_3=l_o-2a} - u_O \tag{24}$$

$$\psi_C = \psi^L\,|_{x_3=l_o-2a} \tag{25}$$

$$w_{C,O} = w^L\,|_{x_3=l_o-2a} - w_O \tag{26}$$

where $u_{C,O}$ and $w_{C,O}$ are the relative displacements of crack tip C to the reference point O in the x and z-directions, respectively, $x_3 = l_o - 2a$ denotes the location of the crack tip C. The displacements, u_O and w_O, of the center reference point O, are determined from the average displacements of the bottom surface of the upper adherend and the top surface of the lower adherend at $x_3 = (l_o\text{-}2a)/2$ as,

$$u_O = \frac{1}{2}\left(u^{oU}\,|_{x_3=(l_o-2a)/2} - \frac{h^U}{2}\psi^U\,|_{x_3=(l_o-2a)/2} + u^{oL}\,|_{x_3=(l_o-2a)/2} + \frac{h^L}{2}\psi^L\,|_{x_3=(l_o-2a)/2} \right) \tag{27}$$

$$w_O = \frac{1}{2}\left(w^U\,|_{x_3=(l_o-2a)/2} + w^L\,|_{x_3=(l_o-2a)/2} \right) \tag{28}$$

If the crack propagates a small length b (virtual crack), the crack tip moves to point C', and the previous crack tip C separates into points A and B, as shown in Figure 4.

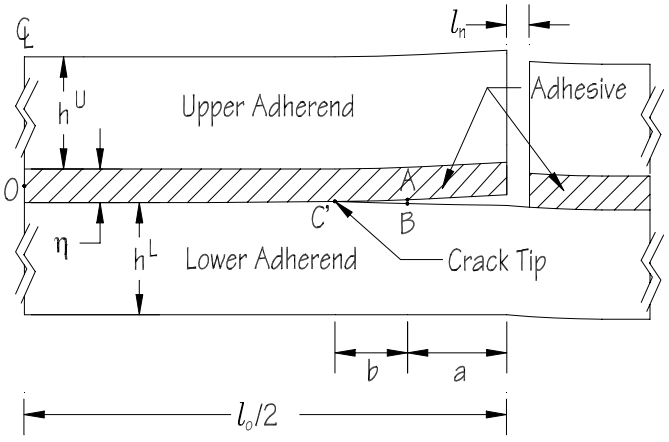

Figure 4. *Virtual crack extension of length b.*

Before the crack growth, the adhesive between *C*' and *C* adheres to the lower adherend where adhesive shear and peel stresses exist at the interface as shown in the left of Figure 5. If the crack propagates a small length *b*, the adhesive shear and peel stresses vanish between *C*' and *C*. The crack tip forces corresponding to a small crack propagation *b* can be assumed as the equivalent forces, N_C, M_C, and Q_C, to the shear and peel stresses between *C'* and *C,* as shown in the right of Figure 5, and can be calculated as

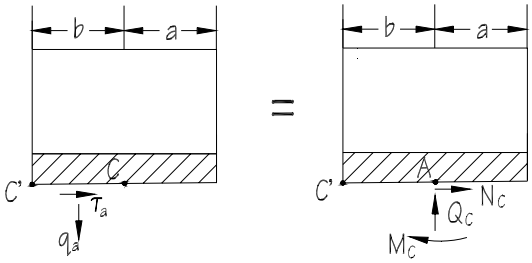

Figure 5. *Equivalent forces at the crack tip.*

$$N_C = \int_{l_o-2a-b}^{l_o-2a} \tau_a dx_3 \tag{29}$$

$$M_C = -\int_{l_o-2a-b}^{l_o-2a} q_a (l_o - 2a - x_3) dx_3 \tag{30}$$

$$Q_C = -\int_{l_o-2a-b}^{l_o-2a} q_a dx_3 \tag{31}$$

where the adhesive shear stress τ_a and peel stress q_a are obtained from the stress model with the overlap length $L_3 = l_o - 2a$. Note that only the upper adherend and adhesive layer with point *A* are shown in Figure 5 and that the positive directions of N_C, M_C, and Q_C are defined to be consistent with the positive directions of displacements *u*, ψ, and *w*, respectively. The same approach is applied to point *B* to obtain the crack tip forces at the lower adherend. It can be seen that the crack tip forces at point *A* have the same magnitude but opposite directions as those at

point *B* because the adhesive stresses acting on the upper adherend are in the opposite directions as those acting on the lower adherend.

After the crack propagates a small length *b*, the previous crack tip *C* separates into two points *A* and *B*, as shown in Figure 4. To determine the relative displacements of point *A* and *B* to the reference point *O*, a subsequent stress analysis is performed using a joint with a central overlap length $L_3 = l_o - 2a - 2b$, which simulates the overlap up to the new crack tip *C'*, including the two notch lengths $L_2 = L_4 = l_n + a + b$. Extension of the upper adherend from *C'* to *A* with a free end at *A* generates the displacements at point *A*. Therefore, the relative displacements of point *A* to the reference point *O* are

$$u_{A,O} = u^{oU}\,|_{x_3=l_o-2a-2b} - \left(\frac{h^U}{2}+\eta\right)\psi^U\,|_{x_3=l_o-2a-2b} - u_O' \tag{32}$$

$$\psi_A = \psi^U\,|_{x_3=l_o-2a-2b} \tag{33}$$

$$w_{A,O} = w^U\,|_{x_3=l_o-2a-2b} + b\frac{dw^U}{dx_3}|_{x_3=l_o-2a-2b} - w_O' \tag{34}$$

The relative displacements of point *B* to point *O* are

$$u_{B,O} = u^{oL}\,|_{x_4=b} + \frac{h^L}{2}\psi^L\,|_{x_4=b} - u_O' \tag{35}$$

$$\psi_B = \psi^L\,|_{x_4=b} \tag{36}$$

$$w_{B,O} = w^L\,|_{x_4=b} - w_O' \tag{37}$$

The subscripts *A* and *B* denote points *A* and *B*. All the other superscripts and subscripts are the same as previously noted. Because of the different joint configuration in the stress model before and after the crack propagates, the displacements of the reference point *O* used in Equations (29) – (34) are obtained again from a stress analysis with a central overlap length $L_3 = l_o - 2a - 2b$ as

$$u_O' = \frac{1}{2}\left(u^{oU}\,|_{x_3=(l_o-2a-2b)/2} - \frac{h^U}{2}\psi^U\,|_{x_3=(l_o-2a-2b)/2} + u^{oL}\,|_{x_3=(l_o-2a-2b)/2} + \frac{h^L}{2}\psi^L\,|_{x_3=(l_o-2a-2b)/2} \right) \quad \textbf{(38)}$$

$$w_O' = \frac{1}{2}\left(w^U\,|_{x_3=(l_o-2a-2b)/2} + w^L\,|_{x_3=(l_o-2a-2b)/2} \right) \quad \textbf{(39)}$$

The central point displacements, u_o and w_o, as shown in Equations (27) and (28) are before the crack propagates and the central point displacements, u_o' and w_o', as in Equations (38) and (39) are after the crack propagates. In order to close the virtual crack propagation, of length b, the crack tip forces are applied on points A and B to move them back to the location of the original crack tip C. Therefore, the total work required to close the small crack propagation b is

$$\begin{aligned} W = {} & \frac{1}{2}\left[N_C\left(u_{C,O} - u_{A,O}\right) + M_C\left(\psi_C - \psi_A\right) + Q_C\left(w_{C,O} - w_{A,O}\right) \right] \\ & - \frac{1}{2}\left[N_C\left(u_{C,O} - u_{B,O}\right) + M_C\left(\psi_C - \psi_B\right) + Q_C\left(w_{C,O} - w_{B,O}\right) \right] \end{aligned} \quad \textbf{(40)}$$

After simplification, the work becomes

$$W = \frac{1}{2}\left[N_C\left(u_{B,O} - u_{A,O}\right) + M_C\left(\psi_B - \psi_A\right) + Q_C\left(w_{B,O} - w_{A,O}\right) \right] \quad \textbf{(41)}$$

For joints with a unit width, the strain energy release rate is defined as the derivative of energy released from the crack propagation with respect to the length of the crack propagation

$$G_T = \frac{dU}{da} \quad \textbf{(42)}$$

where U is the strain energy stored in the body. Based on the VCCT, the total energy released from the crack propagation is equivalent to the work needed to close the same crack propagation. With a virtual crack propagation of length b, the total strain energy release rate G_T, which is a summation of the Mode I strain energy release rate G_I and the Mode II strain energy release rate G_{II}, can be calculated as

$$G_T = G_I + G_{II} = \frac{dU}{da} \cong \frac{W}{b} = \frac{1}{2b}\left[N_C\left(u_B - u_A\right) + M_C\left(\psi_B - \psi_A\right) + Q_C\left(w_A - w_B\right)\right] \quad \textbf{(43)}$$

FINITE ELEMENT MODEL DESCRIPTIONS USING VCCT AND *J*-INTEGRAL METHODS

Finite Element Models using VCCT

The strain energy release rate due to a small increase in crack length is equivalent to the energy required to close that small crack increment. Therefore, the strain energy release rate can be computed by finite element models using the VCCT [15]. As shown in Figure 6, the tip of a crack with an original length *a* is located at *C*. Assuming a virtual crack propagation of length *b*, the new crack tip becomes *C*' and the original crack tip becomes two separate nodes *f* and *g*. If nodes *f* and *g* are restrained at the original crack tip location, this virtual crack with length *b* is closed and the work to close this virtual crack can be calculated by multiplying the reaction forces at nodes *f* and *g* by the relative displacements of these two separate nodes to the original crack tip *C*.

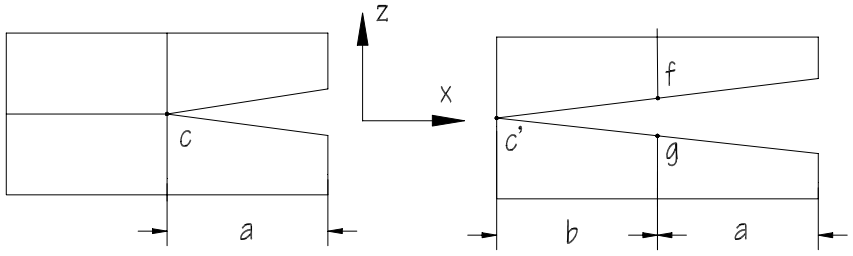

Figure 6. *Demonstration of finite element method with VCCT.*

The virtual crack closure technique originally developed by Rybicki and Kanninen [24] as well as Raju [25] and further developed by Wei [17] is applied in the current study. For 2-D conditions, the following steps are required:

1. Build the finite element model with an original crack of length a and determine the displacements of crack tip C, u_c and w_c in the x and z directions, respectively.
2. Propagate the crack with a small length b (usually one element size); the original crack tip C becomes two separate nodes. Record the displacements of both nodes, u_f, w_f, u_g and w_g.
3. Constrain the two separate nodes so that they have the same displacements as the original crack tip C and obtain the reaction forces F_{xf}, F_{yf}, F_{xg}, and F_{yg}.
4. The work needed to close the virtual crack is

$$W = \frac{1}{2}\left[F_{xf}(u_c - u_f) + F_{yf}(w_c - w_f)\right] + \frac{1}{2}\left[F_{xg}(u_c - u_g) + F_{yg}(w_c - w_g)\right] \quad \textbf{(43)}$$

The total strain energy release rate is then obtained by

$$G_T = \frac{W}{b} \quad \textbf{(44)}$$

In the present study, two-dimensional 4-node linear plane-strain quadrilateral elements are utilized in the finite element model for VCCT application. There are 12 elements through the adherend thickness corresponding to 12 plies of T300/5208 with orientation and sequence of $[0_3/90_3]_S$ and 6 elements are used in the finite element mesh through adhesive thickness.

Finite Element Model Description using the *J*-Integral

Finite element models with the *J*-integral calculation were constructed using ABAQUS™ [21, 22] to verify the present analytical model. The *J*-integral is usually used in quasi-static fracture analysis to characterize the energy release associated with crack propagation. It is equivalent to the strain energy release rate if the material response is linear elastic. Considering

an arbitrary counter-clockwise path (Γ) around the crack tip, as illustrated in Figure 7, the *J*-integral is defined as

$$J = \int_{\Gamma} \left(w dy - \sum_{i=1}^{3} T_i \frac{\partial u_i}{\partial x} ds \right) \qquad \textbf{(45)}$$

where w is the strain energy density, u_1, u_2, and u_3 are the components of the displacement vector, ds is the incremental length along the contour Γ, and T_1, T_2, and T_3 are components of the traction vector. The traction is a stress vector normal to the contour. In other words, T_1, T_2, and T_3 are the normal stresses acting at the boundary if a free-body diagram on the material inside of the contour is constructed.

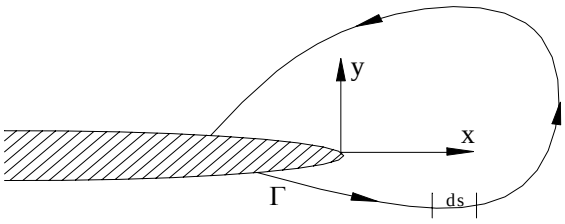

Figure 7. *An arbitrary contour around crack tip.*

Several contour integral evaluations are possible at each location along the crack front. In a finite element model each evaluation can be thought of as the virtual motion of a block of material surrounding the crack tip. Each such block is defined by contours and each contour is a ring of elements completely surrounding the crack tip or crack front from one crack face to the opposite crack face. These rings of elements are defined recursively to surround all previous contours. ABAQUS/Standard automatically finds the elements that form each ring from the node sets given as the crack-tip or crack-front definition. Each contour provides an evaluation of the contour integral [22].

Theoretically, the *J*-integral should be independent of the domain used, but *J*-integral estimated from different rings may vary because of the approximate nature of the finite element solution. Strong variation in these estimates, commonly called domain dependence or contour dependence, indicates a need for mesh refinement (provided that the problem is suitable for contour integrals). Numerical tests suggest that the estimate from the first ring of elements abutting the crack front does not provide a high accuracy result so at least two contours are recommended. In the present study, five contours were calculated and the average was taken as the final *J*-integral value. The method is quite robust in the sense that accurate contour integral estimates are usually obtained even with quite coarse meshes.

Sharp cracks, where the crack faces lie on top of one another in the undeformed configuration, are usually modeled using small-strain assumptions. Focused meshes for *J*-integral calculation, as shown in Figure 8, should normally be used for small-strain fracture mechanics evaluations.

For linear elastic materials, the linear elastic fracture mechanics (LEFM) approach predicts an $r^{-0.5}$ singularity near the crack tip where r is the distance from the crack tip. In finite element analyses, forcing the elements at the crack tip to exhibit an $r^{-0.5}$ strain singularity greatly improves accuracy and reduces the need for a high degree of mesh refinement at the crack tip [26]. This $r^{-0.5}$ singularity can be produced using an eight-node quadrilateral element by moving the mid-side nodes to the quarter-points, as noted by Barsoum [27] and Henshell and Shaw [28]. The needed triangular shape of the elements at the crack tip can be achieved by further collapsing nodes *a*, *b*, and *c*, as shown in Figure 9, while maintaining the $r^{-0.5}$ strain singularity [26]. In the present study, the crack tip was modeled with a ring of collapsed quadrilateral

elements as shown in Figure 9. The procedure used in the finite element analysis is described as follows:

1. Collapse one side of an 8-node element so that all three nodes, *a*, *b*, and *c*, have the same geometric location (on the crack tip).
2. Move the mid-side nodes on the sides connected to the crack tip to the 1/4 point nearest the crack tip.

This procedure will create the strain singularity of $r^{-0.5}$ so it is sufficient for linear elastic fracture analysis.

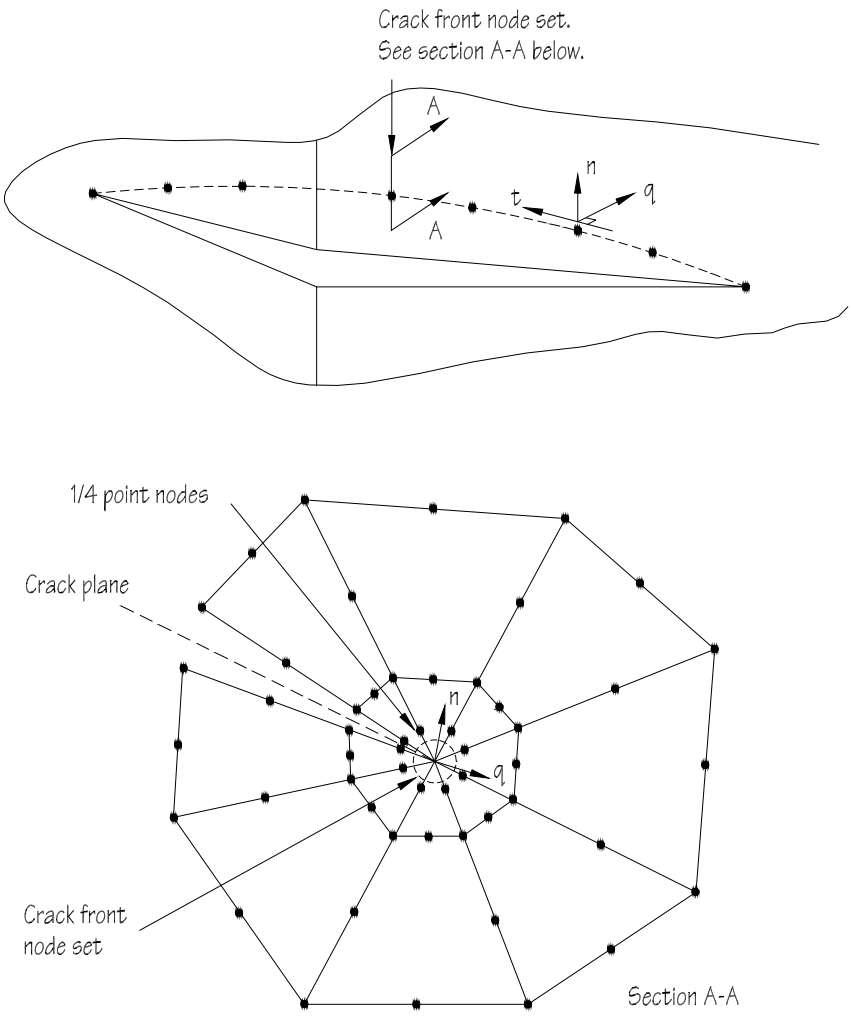

Figure 8. *Typical focused mesh for fracture mechanics evaluation [22].*

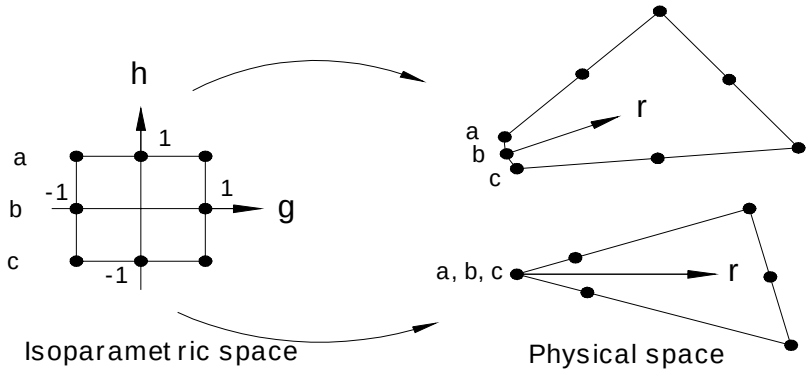

Figure 9. *Collapsed two-dimensional element.*

In the current study, eight-node two-dimensional plane strain elements are used. The crack-tip is meshed using the technique described above to evaluate the *J*-integral. The undeformed and deformed meshes for the ASTM D3165 model are shown in Figure 10. ASTM D3165 and ASTM D1002 configurations are followed to model geometry in the finite element models. Specifically, twelve elements are used through the thickness of the adherends corresponding to twelve plies of T300/5208 with orientation and sequence of $[0_3/90_3]_S$, while five elements are used in the finite element mesh to model the adhesive layer in the thickness direction. The *J*-integral for five different crack lengths and six different loading conditions is evaluated using ABAQUS™ and compared with other models described previously.

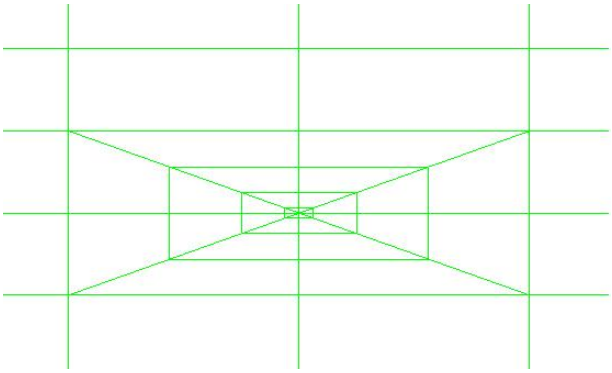

a) Before deformation

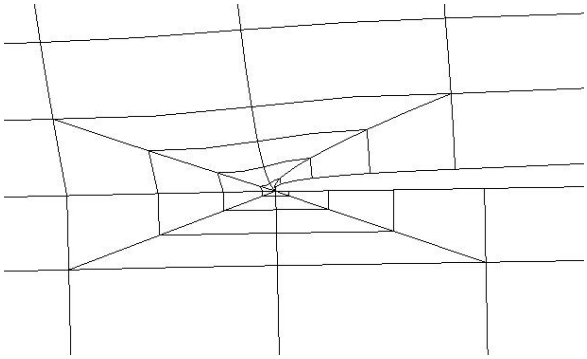

b) After deformation

Figure 10. *Mesh description for the ASTM D3165 model at the singularity interface (for J-integral calculation).*

ASTM D1002 Stress Model

Figure 11 shows the configuration of the ASTM D1002 specimen which is more similar to most field applications. The model derivations of ASTM D1002 specimen configuration are very similar to those for ASTM D3165 specimens. Details can be found in the literature [6]. The general first-order laminated plate equations, Equations (1) – (7), are applied to both the upper and lower adherends. The field equations for Region 1, which is outside of the overlap area, are

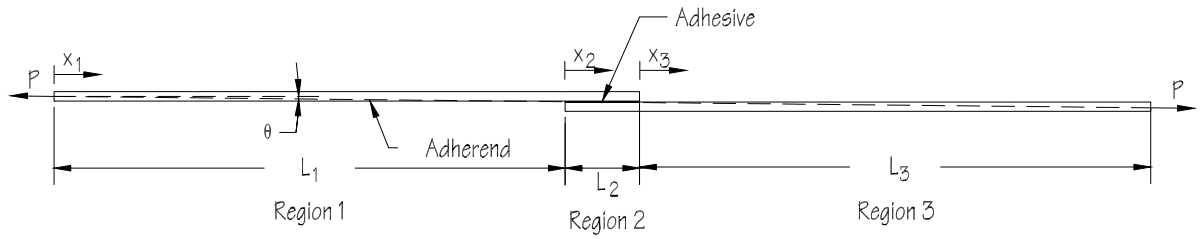

Figure 11. *Configuration of ASTM D1002 specimen.*

$$N_x^U = P \tag{46}$$

$$M_y^U = -P\left(\theta x_1 + w^U\right) \tag{47}$$

$$Q_z^U = -P\left(\theta + \frac{dw^U}{dx_1}\right) \tag{48}$$

and the governing equations for Region 3 are

$$N_x^L = P \tag{49}$$

$$M_y^L = P\left[\theta\left(L_3 - x_3\right) - w^L\right] \tag{50}$$

$$Q_z^L = -P\left(\theta + \frac{dw^L}{dx_3}\right) \tag{51}$$

The oblique angle θ in Equations (47) – (50) is:

$$\theta = \frac{\left(h^U + h^L\right)/2 + \eta}{L_1 + L_2 + L_3} \tag{52}$$

The field equations for Region 2 are the same six second-order ordinary differential equations for ASTM D3165 as shown in Equations (8) – (13). Therefore, the stress model of the ASTM D1002 specimen includes six first-order ordinary differential equations and six second-order ordinary differential equations with 12 variables. A total of 18 boundary conditions are obtained at the two ends of each region from either continuity or applied force conditions [6]. The symbolic solver Maple 9 is used to solve the system of equations. The strain energy release rate is calculated with the similar VCCT procedures as described in previous section regarding ASTM D3165 specimens.

RESULTS AND DISCUSSION

In the present study, both ASTM D3165 and ASTM D1002 were modeled analytically to determine the strain energy release rate using the methods described previously. The symbolic solver Maple 9 was utilized as the mathematical tool. The finite element models for VCCT and *J*-integral were conducted using ABAQUS™ to verify the analytical results.

In order to demonstrate the application of the developed model, T300/5208 (Graphite/Epoxy) with ply thickness of 0.25 mm was used for both upper and lower adherends. Each adherends consist of 12 plies with orientation and sequence of $[0_3/90_3]_S$. The engineering constants of T300/5208 are E_{11} = 181 GPa, E_{22} = 10.3 GPa, G_{12} = 7.17 GPa, and v_{12} = 0.28. For convenience, other mechanical properties of the adherends are assumed as

$E_{33} = E_{22}$, $G_{13} = G_{12}$, $v_{13} = v_{12}$, v_{23} = 0.35, and $G_{23} = E_{22}/(2+ 2v_{23})$ = 3.815 GPa

The adhesive is Metbond 408 with the following properties:

$$E_a = 0.96 \text{ GPa} \qquad G_a = 0.34 \text{ GPa} \qquad v_a = 0.41$$

The joint dimensions of the ASTM D3165 specimen include the central overlap length l_o = 30 mm, notch size l_n = 1.6 mm, and adherend lengths outside the central overlap $L_1 = L_5$ = 78.4 mm, and adhesive thickness η = 0.2 mm. The joint dimensions of the ASTM D1002 specimen include an overlap length of l_o = 30 mm and adherend lengths outside the overlap $L_1 = L_3$ = 80 mm, which includes the gripped portion of the specimen.

When a load P = 1,000 N/m was applied, the adhesive peel and shear stresses obtained from both the semi-analytical model and finite element model are shown in Figures 12 and 13 for ASTM D3165 specimens and in Figures 14 and 15 for ASTM D1002 specimens, respectively. Because of symmetry, only half of the overlap region is shown in the figures. It can be seen from the figures that the semi-analytical solutions and finite element results are very close, except in the vicinity of the edge (x_3 = 30 mm). This is because the adhesive is assumed to behave as an elastic material and the adhesive stress distributions are defined as being uniform through the thickness in the derivation. In a real joint, the adhesive would undergo plastic deformations and the stress at the joint ends would be reduced.

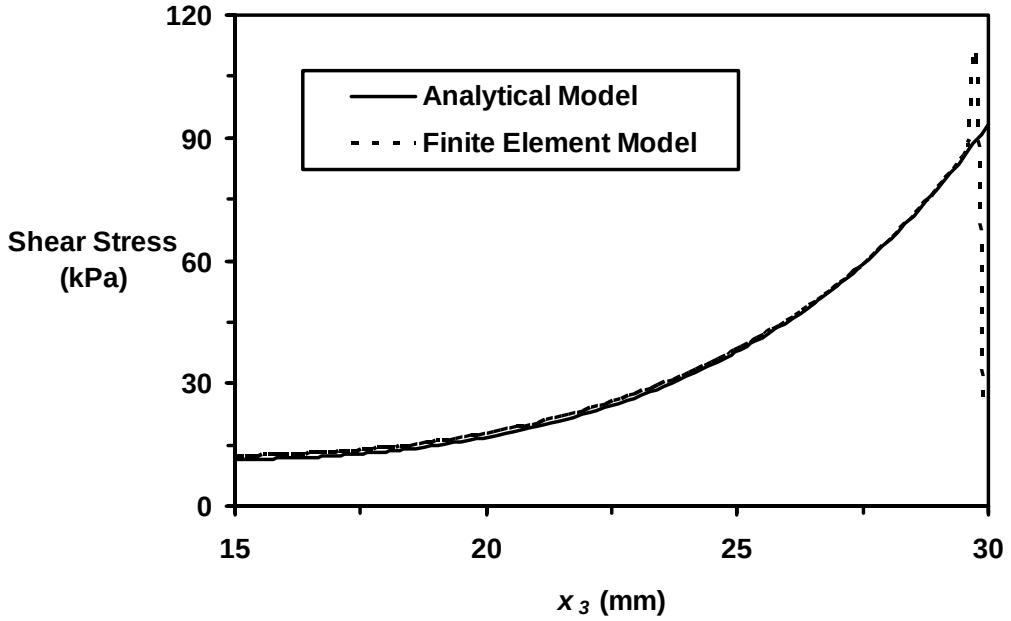

Figure 12. *Adhesive shear stress distribution in Region 3 for the ASTM D3165 specimen.*

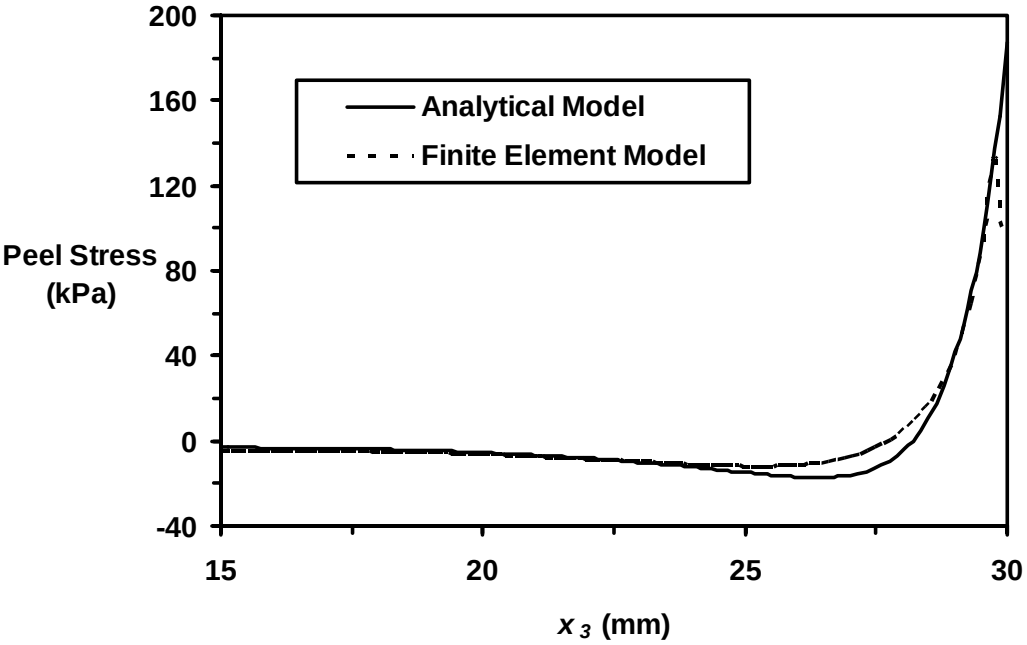

Figure 13. *Adhesive peel stress distribution in Region 3 for the ASTM D3165 specimen.*

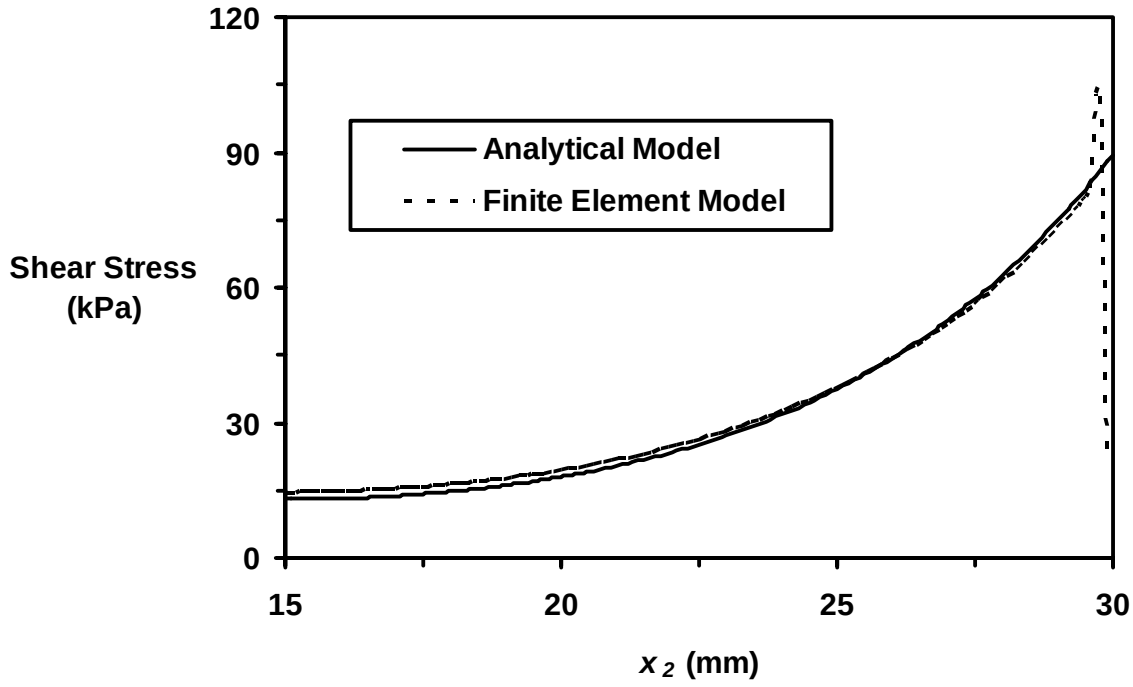

Figure 14. *Adhesive shear stress distribution in Region 2 for the ASTM D1002 specimen.*

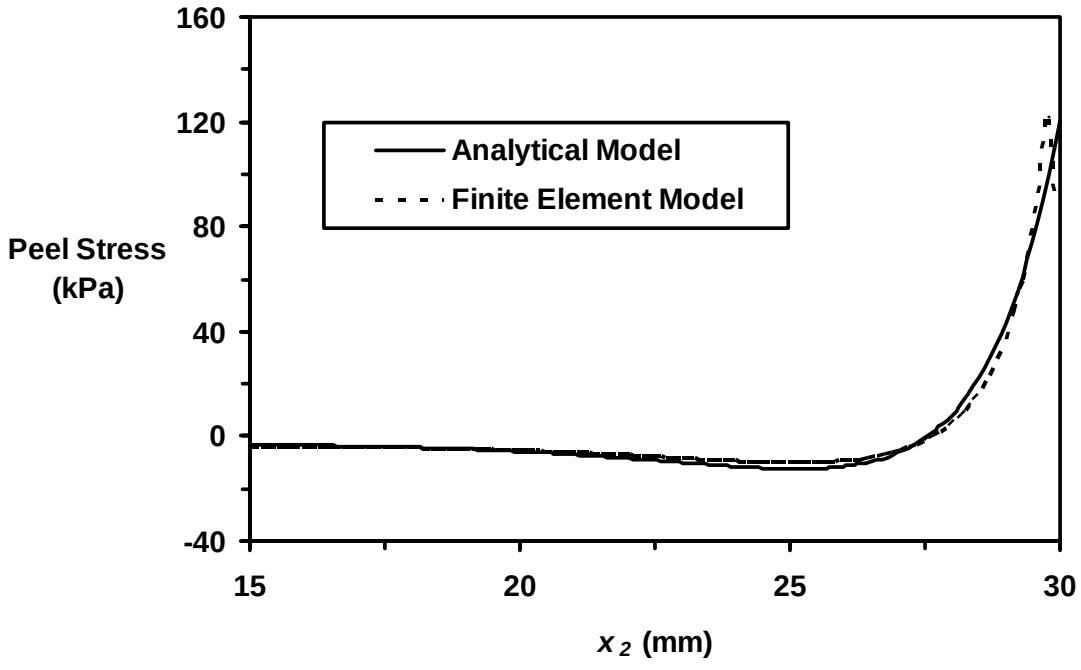

Figure 15. *Adhesive peel stress distribution in Region 2 for the ASTM D1002 specimen.*

Once the stress, strain, and displacement fields were obtained, the strain energy release rates of the joints were estimated and the solutions from the semi-analytical models using the VCCT were compared with finite element models using the VCCT and finite element models using the *J*-integral. The strain energy release rates for five different crack lengths (a = 0.15 mm, 1.5 mm, 3 mm, 6 mm, and 9 mm) under tensile load P = 200 kN/m are shown in Figures 16 and 17 for ASTM D3165 and D1002 specimen geometries, respectively. It can be seen that results from finite element models with the VCCT and *J*-integral are almost identical while the developed semi-analytical model deviates about 10% from the finite element models for the ASTM D3165 specimen. For the ASTM D1002 geometry, all three models provided almost identical strain energy release rates except for a very short pre-crack. The strain energy release rates with crack length a = 3 mm under various loads are shown in Figures 18 and 19 for ASTM D3165 and D1002 specimen geometries, respectively. As expected, the strain energy release rates from all three models appear to be quadratic functions of the applied load. The semi-analytical results correlate very well for the models with the ASTM D1002 specimen geometry.

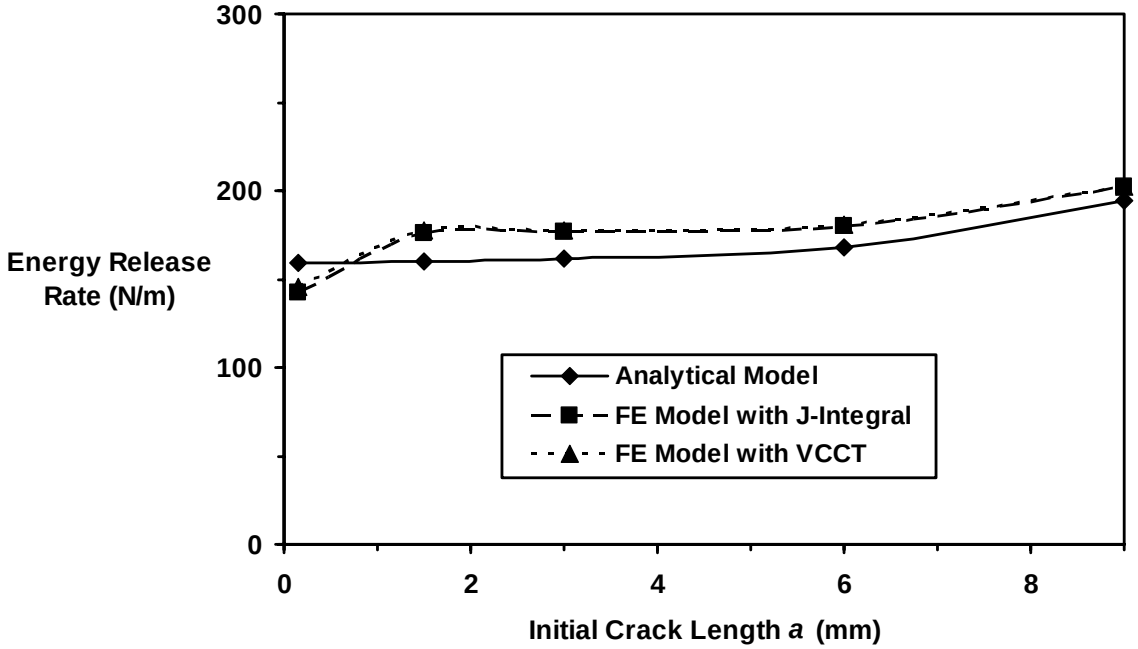

Figure 16. *Strain energy release rate of an ASTM D3165 specimen as a function of initial crack length.*

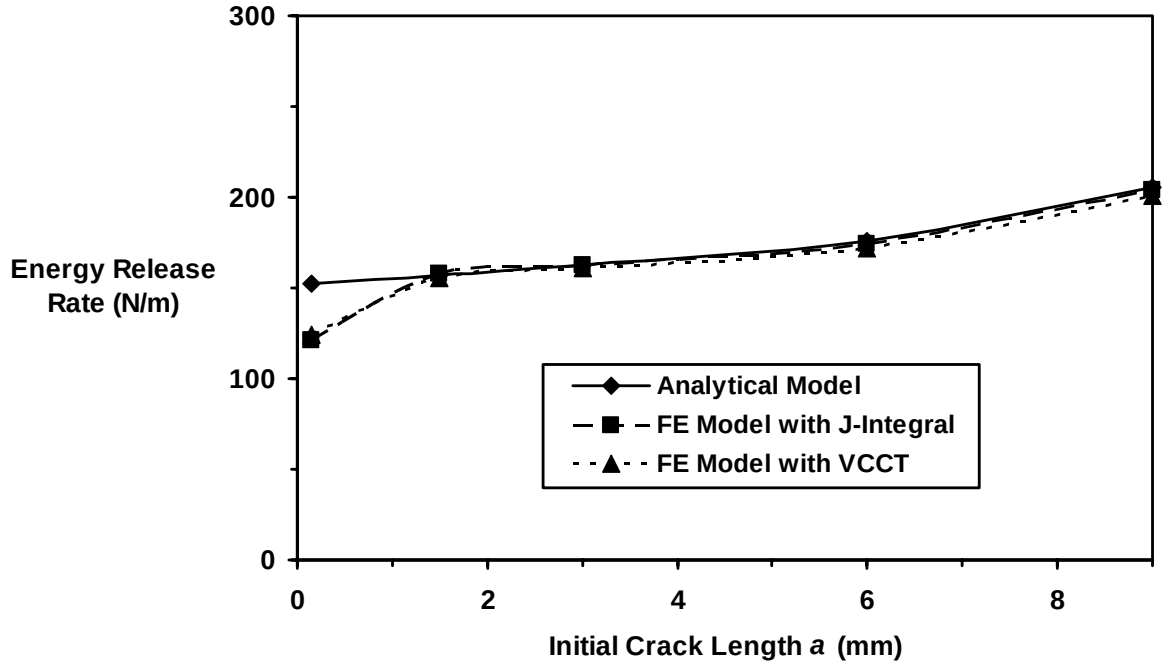

Figure 17. *Strain energy release rate of an ASTM D1002 specimen as a function of initial crack length.*

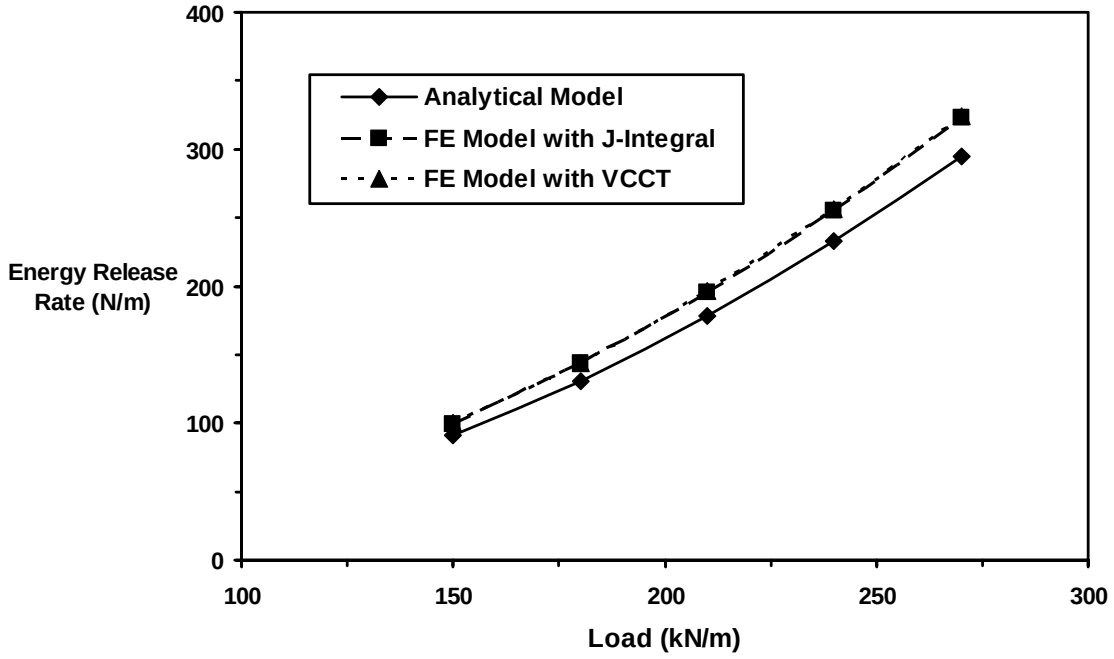

Figure 18. *Strain energy release rate of an ASTM D3165 specimen as a function of load.*

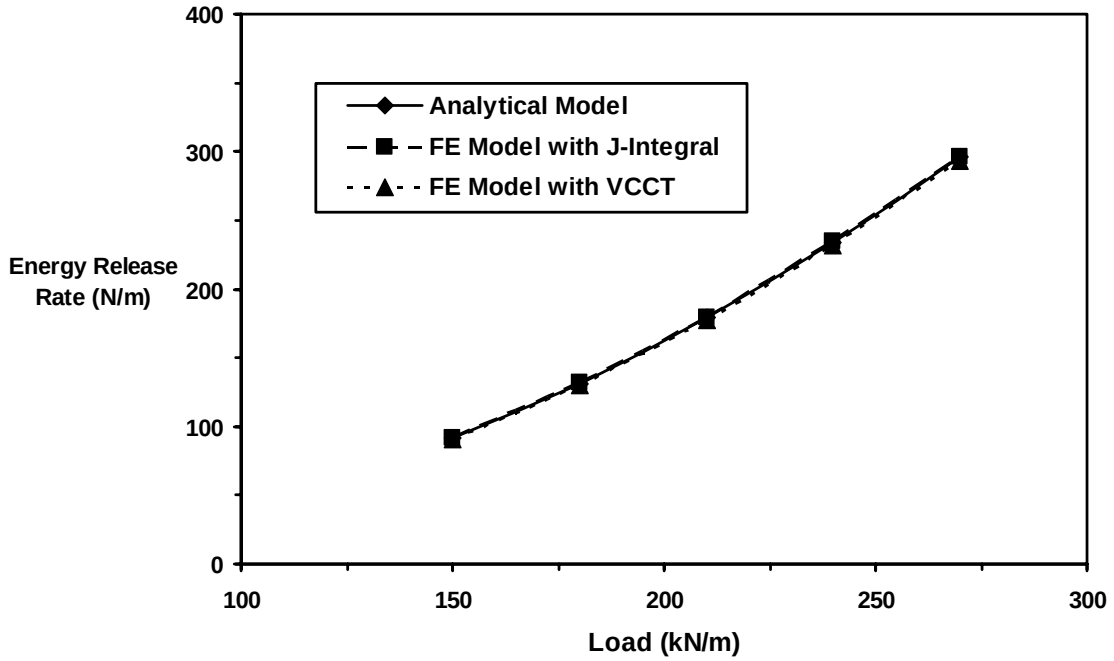

Figure 19. *Strain energy release rate of an ASTM D1002 specimen as a function of load.*

CONCLUSION

A semi-analytical method was developed to calculate the strain energy release rate based on ASTM D3165 and D1002 specimen geometries with a prescribed interface crack. The stress and displacement fields for the adhesively-bonded single-lap composite joint were determined based on laminated anisotropic plate theory. The virtual crack closure technique (VCCT) was applied effectively in conjunction with the analytical stress and displacement models in determining the strain energy release rate. Results obtained from the developed semi-analytical method correlated well with results from finite element models using both the VCCT and *J*-integral. Therefore, the present study has given a description of a reasonably accurate, rapid-solution method for calculating the strain energy release rate of an adhesively-bonded single-lap composite joint. Strength predictions of representative joints are anticipated by using the critical strain energy release rate of the adhesive/adherend interface from the developed method.

ACKNOWLEDGMENTS

This study was partially supported by NASA Langley Research Center under contract number NAS1-03056. The support of the NSF under Grant No. EIA-0216178 and Grant No. EPS-0236913, and matching support from the State of Kansas and the Wichita State University High Performance Computing Center are also acknowledged.

REFERENCES

1. Yang, C., Tomblin, J. S., and Guan, Z., "Analytical Modeling of ASTM Lap Shear Adhesive Specimens," Technical Report, DOT/FAA/AR-02/130, February 2003.

2. Kutscha, D., "Mechanics of Adhesive-Bonded Lap-Type Joints: Survey and Review," Technical Report AFML-TDR-64-298, 1964.

3. Kutscha, D. and Hofer, K. E., Jr., "Feasibility of Joining Advanced Composite Flight Vehicles," Technical Report AFML-TR-68-391, 1969.

4. Matthews, F. L., Kilty, P. F., and Goodwin, E. W., "A Review of the Strength of Joints in Fibre-Reinforced Plastics: Part 2 Adhesively Bonded Joints," *Composites*, Vol. 29, 1982.

5. Vinson, J. R., "Adhesive Bonding of Polymer Composites," Polymer Engineering and Science, Vol. 29, pp. 1325, 1989.

6. Yang, C., and Pang, S. S., "Stress-Strain Analysis of Single-Lap Composite Joints under Tension," ASME Transaction, *Journal of Engineering Materials and Technology*, Vol. 118, pp. 247-255, 1996.

7. Huang, H., Yang, C., Tomblin, J.S., and Harter, P., "Stress and Failure Analyses of Adhesive-Bonded Composite Joints using ASTM D3165 Specimens," *ASTM Journal of Composites Technology & Research*, Vol. 24, No. 2, pp. 345-356, 2002.

8. Yang, C., Huang, H., Tomblin, J. S., and Sun, W., "Elastic-plastic Model of Adhesive-bonded Single-lap Composite Joints," *Journal of Composite Materials*, Vol. 38, No. 4, pp. 293-309, 2004.

9. Krueger, D., "The Virtual Crack Closure Technique: History, Approach and Applications," Technical Report, NASA/CR-2002-211628, ICASE Report No. 2002-10, April 2002.

10. Schapery, R. A. and Davidson, B. D., "Prediction of Energy Release Rate for Mixed-mode Delamination using Classical Plate Theory," *Applied Mechanics Review*, Vol. 43, No. 5, Part 2, 1990.

11. Davidson, B. D., "Prediction of Energy Release Rate for Edge Delamination Using a Crack Tip Element Approach," *Composite Materials: Fatigue and Fracture-Fifth Volume*, pp.155-175, 1995.

12. Davidson, B. D., Hu, H., and Schapery, R. A., "An analytical Crack-Tip Element for Layered Elastic Structures," *Journal of Applied Mechanics*, Vol. 62, pp. 294-305, 1995.

13. Davidson, B. D., Yu, L., and Hu, H., "Delamination of Energy Release Rate and Mode Mix in Three-dimensional Layered structures Using Plate Theory," *International Journal of Fracture*, Vol. 105, pp. 81-104, 2000.

14. Park, O. and Sankar, B. V., "Crack-tip Force Method for Computing Energy Release Rate in Delaminated Plates," *Composite Structures*, Vol. 55, pp. 429-434, 2002.

15. Kim, I.-G. and Kong, C.-D., "Generalized Theoretical Analysis Method for Free-edge Delaminations in Composite Laminates," *Journal of Materials Science*, Vol. 37, pp. 1875-1880, 2002.

16. Wang, J. T., Xue, D. Y., Sleight, D. W., and Housner, J. M., "Computation of Energy Release Rate for Cracked Composite Panels with Nonlinear Deformation," AIAA/ASME/ASCE/AHS/ASC Structures, Structural Dynamics & Materials Conference, No. 4, pp. 2713-2727, 1995.

17. Wei, Y., Yang, T., Wan, Z., and Du, X., "New VCCT and Its Application in Composite Delamination Analysis," *Chinese Journal of Computational Mechanics*, Vol. 17, No. 3, pp. 308-312, 2000.

18. "Strength Properties of Adhesives in Shear by Tension Loading of Single-lap-joint Laminated Assemblies," ASTM D3165-95.

19. "Standard Method of Test for Strength Properties of Adhesives in Shear by Tension Loadings (Metal-to-Metal)," ASTM D1002-72.

20. Maple 9 Advanced Programming Guide, Materloo Maple Inc., Waterloo, Canada, 2003.

21. *ABAQUS/CAE User's Manual*, Version 6.3, Hibbitt, Karlsson & Sorensen, Inc., 2002.

22. *ABAQUS/Standard User's Manual*, Version 6.3, Hibbitt, Karlsson & Sorensen, Inc., 2002.

23. Whitney, J. M., *Structural Analysis of Laminated Anisotropic Plates*, Technomic Publishing Company, Inc., Lancaster, PA, 1987.

24. Rybicki, E. F. and Kanninen, M.F., "A Finite Element Calculation of Stress Intensity Factors by a Modified Crack Closure Integral," *Engineering Fracture Mechanics*, Vol. 9, pp. 931-938, 1977.

25. Raju, I. S., "Calculation of Strain-Energy Release Rates With Higher Order And Singular Finite Elements," *Engineering Fracture Mechanics*, Vol. 28, pp. 251-274, 1987.

26. Anderson, T. L., *Fracture Mechanics: Fundamentals and Applications*, second edition, CRC Press LLC, Boca Raton, FL, 1995.

27. Barsoum, R. S., "On the Use of Isoparametric Finite Elements in Linear Fracture Mechanics," *International Journal for Numerical Methods in Engineering*, Vol. 10, pp. 25-37, 1976.

28. Henshell, R. D. and Shaw, K. G., "Crack Tip Finite Elements are Unnecessary," *International Journal for Numerical Methods in Engineering*, Vol. 9, pp. 495-507, 1975.